



1 **Relative humidity-dependent viscosity of secondary organic**  
2 **material from toluene photo-oxidation and possible**  
3 **implications for organic particulate matter over megacities**

4

5 M. Song<sup>1,2</sup>, P. F. Liu<sup>3</sup>, S. J. Hanna<sup>1</sup>, R. A. Zaveri<sup>4</sup>, K. Potter<sup>5</sup>, Y. You<sup>1</sup>, S. T. Martin<sup>3,6</sup>, A.  
6 K. Bertram<sup>1</sup>

7 [1] {Department of Chemistry, University of British Columbia, Vancouver, BC, V6T 1Z1, Canada}

8 [2] {Department of Earth and Environmental Sciences, Chonbuk National University, Jeollabuk-  
9 do, Republic of Korea}

10 [3]{John A. Paulson School of Engineering and Applied Sciences, Harvard University, Cambridge,  
11 Massachusetts 02138, USA}

12 [4]{Atmospheric Sciences and Global Change Division, Pacific Northwest National Laboratory,  
13 Richland, WA, USA}

14 [5]{School of Chemistry, University of Bristol, Bristol, UK BS8 1TS, UK}

15 [6]{Department of Earth and Planetary Sciences, Harvard University, Cambridge, Massachusetts  
16 02138, USA}

17 Correspondence to: A. K. Bertram (bertram@chem.ubc.ca)

18

19 **Abstract**

20 To improve predictions of air quality, visibility, and climate change, knowledge of the viscosities  
21 and diffusion rates within organic particulate matter consisting of secondary organic material  
22 (SOM) is required. Most qualitative and quantitative measurements of viscosity and diffusion rates  
23 within organic particulate matter have focused on SOM particles generated from biogenic VOCs  
24 such as  $\alpha$ -pinene and isoprene. In this study, we quantify the relative humidity (RH)-dependent  
25 viscosities at  $295 \pm 1$  K of SOM produced by photo-oxidation of toluene, an anthropogenic VOC.



1 The viscosities of toluene-derived SOM were  $2 \times 10^{-1}$  to  $\sim 6 \times 10^6$  Pa·s from 30 to 90% RH, and  
2 greater than  $\sim 2 \times 10^8$  Pa·s (similar to or greater than the viscosity of tar pitch) for  $\text{RH} \leq 17\%$ . These  
3 viscosities correspond to Stokes-Einstein-equivalent diffusion coefficients for large organic  
4 molecules of  $\sim 2 \times 10^{-15}$   $\text{cm}^2 \cdot \text{s}^{-1}$  for 30% RH, and lower than  $\sim 3 \times 10^{-17}$   $\text{cm}^2 \cdot \text{s}^{-1}$  for  $\text{RH} \leq 17\%$ .  
5 Based on these estimated diffusion coefficients, the mixing time of large organic molecules within  
6 200 nm toluene-derived SOM particles is 0.1 - 5 hr for 30% RH, and higher than  $\sim 100$  hr for  $\text{RH}$   
7  $\leq 17\%$ . These results were used, as a first-order approximation, to estimate if organic particulate  
8 matter will be in well-mixed over the world's top 15 most populous megacities. If the organic  
9 particulate matter in the megacities is similar to the toluene-derived SOM in this study, in Kolkata,  
10 Istanbul, Dhaka, Tokyo, Shanghai, and Mumbai, mixing times in organic particulate matter during  
11 extended periods of the year will be very short, and well-mixed particles can be assumed. On the  
12 other hand, the mixing times of large organic molecules in organic particulate matter in Delhi,  
13 Beijing, Mexico City, Cairo, and Karachi may be long and the particles may not be well-mixed in  
14 the afternoon (3:00 – 5:00 local time) during certain times of the year.

15

## 16 **1 Introduction**

17 Volatile organic compounds (VOCs) are released into the atmosphere from both biogenic and  
18 anthropogenic sources. In the atmosphere, VOCs can form secondary organic material (SOM)  
19 through oxidation reactions with OH radicals,  $\text{NO}_3$  radicals, and  $\text{O}_3$ . SOM accounts for 20 – 80%  
20 of the mass of organic atmospheric particulate matter at various locations (Zhang et al., 2007;  
21 Jimenez et al., 2009). SOM typically consist of thousands of different compounds, and only 10 –  
22 20% of the individual molecules that make up SOM particles have been identified (Decesari et al.,  
23 2006; Hallquist et al., 2009). The lack of information on the chemical composition of SOM has  
24 resulted in a poor understanding of their physical properties, including the viscosity and molecular  
25 diffusion rates within SOM particles.

26 Knowledge of the viscosity and molecular diffusion rates within SOM particles is needed to predict  
27 the properties of these particles and understand their role in the atmosphere. For example, the size  
28 distribution and mode diameter depend on the diffusion rates of organic molecules within the  
29 particles (Riipinen et al., 2011; Zaveri et al., 2014). Simulations show that total SOM mass



1 concentrations can be overestimated or underestimated depending on what diffusion rates are used  
2 (Shiraiwa and Seinfeld, 2012). Chemical aging of atmospheric particles by heterogeneous  
3 reactions can depend on diffusion rates within SOM (Shiraiwa et al., 2011; Kuwata and Martin,  
4 2012; Zhou et al., 2013; Steimer et al., 2014; Houle et al., 2015) and heterogeneous ice nucleation  
5 may be influenced by the viscosity of SOM particles (Murray et al., 2010; Wang et al., 2012;  
6 Ladino et al., 2014; Schill et al., 2014; Wilson et al., 2012). Moreover, long-range transport of  
7 polycyclic aromatic hydrocarbons can depend on diffusion rates in a particle (Zelenyuk et al., 2012;  
8 Zhou et al., 2013) and the efflorescence of crystalline salts can be hindered for highly viscous  
9 SOM (Murray, 2008; Murray and Bertram, 2008; Bodsworth et al., 2010; Song et al., 2013).

10 Most qualitative and quantitative measurements of viscosity and diffusion rates within organic  
11 particulate matter have focused on SOM generated from biogenic VOCs such as  $\alpha$ -pinene and  
12 isoprene (Virtanen et al., 2010; Cappa et al., 2011; Perraud et al., 2012; Saukko et al., 2012;  
13 Abramson et al., 2013; Robinson et al., 2013; Renbaum-Wolff et al., 2013a; Bateman et al., 2015;  
14 Kidd et al., 2014; Pajunoja et al., 2014; Wang et al., 2014; Song et al., 2015). Recently, the  
15 viscosity and diffusion rates within SOM particles generated from anthropogenic VOCs have also  
16 been investigated. Using single particle mass spectrometry, Robinson et al. (2013) investigated  
17 mixing of toluene-derived SOM particles and SOM particles from  $\alpha$ -pinene ozonolysis. One  
18 possible explanation of the lack of mixing within toluene-derived SOM particles was a high  
19 viscosity of the SOM. From bounce experiments, Saukko et al. (2012) reported that SOM particles  
20 derived from naphthalene and n-heptadecane are highly viscous upon increasing oxidation. Also  
21 from bounce experiments, Bateman et al. (2015) showed SOM derived from photo-oxidation of  
22 toluene had a viscosity  $> 100 \text{ Pa}\cdot\text{s}$  for relative humidity (RH) values  $< 80\%$ . Li et al. (2015)  
23 showed through bounce experiments that SOM derived from *m*-xylene and 1,3,5-trimethylbenzene  
24 had a viscosity of  $> 100 \text{ Pa}\cdot\text{s}$  at RH values less than 70%. Li et al. (2015) also used results of  
25 reactive uptake studies to infer that for RH values of 35 - 45% the diffusion coefficient of  
26 carboxylic acids within SOM generated from several anthropogenic VOCs (toluene, *m*-xylene and  
27 1,3,5-trimethylbenzene) was  $3 \times 10^{-18} \pm 0.5 \text{ m}^2 \text{ s}^{-1}$ . Although there has been recent progress in  
28 measuring the viscosity and diffusion rates within SOM generated from anthropogenic VOCs,  
29 additional studies are needed to quantify the viscosities and diffusion rates over the full range of  
30 RH found in the atmosphere.



1 In the following, we measure the viscosities of toluene-derived SOM over the range of RH values  
2 found in the atmosphere. As in previous studies, SOM from the photo-oxidation of toluene serves  
3 as a proxy for organic particulate matter from anthropogenic sources in megacities (e.g. Pandis et  
4 al., 1992; Robinson et al., 2013). After determining viscosities as a function of RH, the Stokes-  
5 Einstein equation is used to convert the viscosities into equivalent diffusion rates of large organic  
6 molecules within toluene-derive SOM. The Stokes-Einstein equation should give reasonable  
7 values of diffusion rates when the viscosity is not near the viscosity of a glass ( $\sim 10^{12}$  Pa s) and  
8 when the molecules are roughly the same size or larger than the molecules in the SOM matrix  
9 (Champion et al., 2000; Koop et al., 2011; Shiraiwa et al., 2011; Power et al., 2013). Finally, the  
10 results are used to estimate the viscosities and diffusion rates in organic particulate matter over  
11 megacities.

12

## 13 **2 Experimental**

14 The production and collection of SOM particles onto hydrophobic substrates (which are needed  
15 for the beam mobility and poke-and-flow experiments) is discussed in Sect. 2.1. The viscosity of  
16 toluene-derived SOM was determined using the bead-mobility technique and the poke-flow  
17 technique together with simulations of fluid flow. These two techniques are discussed in Sects. 2.2  
18 and 2.3.

### 19 **2.1 Production and collection of secondary organic material on hydrophobic** 20 **substrates**

21 SOM aerosols particles having diameters less than 1  $\mu\text{m}$  were generated by toluene photo-  
22 oxidation in an oxidation flow reactor (OFR) (Kang et al., 2007; Lambe et al., 2011). The  
23 procedure for generating SOM from toluene photo-oxidation in the flow reactor has been given by  
24 Liu et al. (2013). Only the details relevant to the current experiments are given here.

25 For this study, the volume of the OFR was 13.3 L and the reactor was operated at a flow rate of  
26  $\sim 7 \text{ L m}^{-1}$  with a residence time in the range of  $\sim 110$  s. The temperature used in the OFR  
27 experiments was  $293 \pm 2$  K and the concentrations of toluene and ozone used in the flow reactor  
28 are listed in Table 1. Ozone was produced external to the flow reactor by irradiating pure air with



1 the ultraviolet emission from an Hg lamp ( $\lambda = 185$  nm). The injected ozone concentration was ~30  
2 ppm. Hydroxyl radicals were produced inside the OFR by the following photochemical reactions:



5 Mass concentrations of SOM particles in the OFR were 60-100  $\mu\text{g m}^{-3}$  and 600-1000  $\mu\text{g m}^{-3}$  for  
6 the two different experimental conditions (see Table 1). At the outlet of the OFR, two different  
7 methods were used for the collection of SOM particles. In the first method, SOM particles were  
8 collected on a hydrophobic slide using an electrostatic precipitator (TSI 3089, USA). After  
9 collection, the SOM particles on the hydrophobic slides, formed from coalescence during sampling,  
10 were smaller than ~5  $\mu\text{m}$  in diameter. For the bead-mobility and poke-flow techniques, however,  
11 particle sizes between 20 - 60  $\mu\text{m}$  in diameter are needed. To generate these large sizes, the  
12 hydrophobic slides containing the SOM particles were placed inside an RH- and temperature-  
13 controlled flow cell (Pant et al., 2006; Bertram et al., 2011; Song et al., 2012) and the RH was  
14 increased to > 100%. This procedure caused particle growth by water uptake and eventual  
15 coagulation among particles. This growth and coagulation process resulted in larger but fewer  
16 SOM particles on the hydrophobic slides. Details of this procedure are given by Renbaum-Wolff  
17 et al. (2015) and Song et al. (2015). This procedure was used for samples 1, 2, 5, and 6 shown in  
18 Table 1.

19 In the second method, SOM particles were collected on hydrophobic surfaces using a single stage  
20 impactor (Prenni et al., 2009; Poschl et al., 2010). During impaction, the collected submicron SOM  
21 particles coagulated, resulting in particles with sizes between 10 and 100  $\mu\text{m}$  in diameter. These  
22 supermicron particles were used directly in the bead-mobility and poke-flow experiments. This  
23 procedure was used to collect samples 3, 4, 7, and 8 shown in Table 1.

24 For all the bead-mobility experiments, a Teflon substrate was used. For all the poke-and-flow  
25 experiments, hydrophobic glass slides coated with trichloro(1*H*,1*H*,2*H*,2*H*-perfluorooctyl)silane  
26 (Sigma-Aldrich) were used. The coating procedure is described in Knopf (2003).

## 27 **2.2 Bead-mobility experiments**



1 The bead-mobility technique was previously described in Renbaum-Wolff et al. (2013a, b). Briefly,  
2 a water suspension of  $\sim 1 \mu\text{m}$  insoluble melamine beads (Sigma Aldrich Cat. #86296) was  
3 nebulized and incorporated into supermicron SOM particles deposited on a hydrophobic substrate  
4 (toluene samples 1-4, Table 1). The hydrophobic substrate with the SOM particles and beads was  
5 placed in a flow-cell with variable RH and a temperature of  $295 \pm 1 \text{ K}$ . A continuous flow of  
6  $\text{N}_2/\text{H}_2\text{O}$  gas (flow rate  $\approx 1200 \text{ sccm}$ ) was passed over the supermicron particles. The flow above  
7 the particles resulted in a shear stress on the particle surface and internal circulations within the  
8 particle, which could be visualized by observing the beads within the particles with a light-  
9 transmitting microscope coupled to a CCD camera (Zeiss Axio Observer, magnification  $40\times$ ).  
10 Figure 1 shows images from a typical bead-mobility experiment for a toluene-derived SOM  
11 particle at 80% RH. Typically, 1 to 7 beads were monitored within a particle over 50 - 100 frames.  
12 The time between frames ranged from 0.2 s – 10 min depending on the velocity of the beads. From  
13 the location of the beads as a function of time, the speed of individual beads was determined. These  
14 individual speeds were then used to determine average bead speeds for a given sample and RH.  
15 The measured speeds of 3 - 10 beads were used to determine a mean bead speed. Bead speeds were  
16 not reported at  $\text{RH} < 60\%$  since at these RH values the movements of the beads were too slow to  
17 measure for typical observation times.

18 The average bead speed for a given sample and RH was converted to viscosity using a calibration  
19 line. The calibration line was developed by Song et al. (2015) from measurements of bead speed  
20 in sucrose-water particles over a range of RH values. The RH within the flow-cell was measured  
21 using a hygrometer with a chilled mirror sensor (General Eastern, Canada), which was calibrated  
22 by measuring the deliquescence RH for pure ammonium sulfate particles (80.0% RH at 293 K,  
23 Martin (2000)). The uncertainty of the hygrometer was  $\pm 0.5\%$  RH after calibration.

### 24 **2.3 Poke-flow technique in conjunction with fluid simulation**

25 The poke-and-flow technique in conjunction with fluid simulations was used to measure the  
26 viscosities of SOM particles at RH values less than 50%. This technique was not used at RH values  
27  $> 50\%$  since the flow rates of the SOM after poking were too fast to observe at these RH values.  
28 The qualitative method of poking an inorganic particle to determine its phase (i.e., solid or liquid)  
29 was introduced by Murray et al. (2012). Renbaum-Wolff et al. (2013a) and Grayson et al. (2015a)  
30 expanded on this method by measuring the characteristic flow time of a material after poking and



1 extracting viscosity information from simulations of fluid flow. Briefly, supermicron toluene-  
2 derived SOM particles deposited on a hydrophobic substrate (Toluene 5 to 8, Table 1) were placed  
3 inside a flow-cell with RH control. The particles were conditioned for 30 min at > 70% RH, 60  
4 min at 60 – 70% RH, 2 h at 30 – 60% RH, and 3 h at  $\leq$  30% RH. These times are sufficient for the  
5 particles to equilibrate with the surrounding water vapor based on recent measurements of  
6 diffusion coefficients of water within SOM (Price et al., 2015). After equilibration, particles were  
7 poked using a sharp needle (0.9 mm  $\times$  40 mm) (Becton-Dickson, USA) that was mounted to a  
8 micromanipulator (Narishige, model MO-202U, Japan) and inserted through a small hole in the  
9 top of the flow-cell. The geometrical changes before, during, and after poking a particle were  
10 recorded by a reflectance optical microscope (Zeiss Axio Observer, 40 $\times$  objective) equipped with  
11 a CCD camera. At 30 - 50% RH the action of poking the particles with the needle resulted in the  
12 material forming a half torus geometry (see Fig. 2a). From the images recorded after poking the  
13 particles, the experimental flow time,  $\tau_{\text{exp, flow}}$ , was determined. The experimental flow time was  
14 defined as the time taken for the equivalent-area diameter of the inside of the half torus geometry  
15 to reduce to 50% of the initial diameter. Here the equivalent-area diameter,  $d$ , is calculated as  $d =$   
16  $(4A/\pi)^{1/2}$  where  $A$  represents the hole area (Reist, 1992). For RH < 20% the SOM particles shattered  
17 after poking, and no restorative flow was observed over  $\sim$ 5 hr (See Fig. 2b). In this case  $\tau_{\text{exp, flow}}$   
18 was set to > 5 hr.

19 To determine viscosities from  $\tau_{\text{exp, flow}}$ , simulations of fluid flow were carried out with the finite-  
20 element analysis software package, *COMSOL Multiphysics* (Renbaum-Wolff et al., 2013a;  
21 Grayson et al., 2015a). The mesh size used in the simulations was 4.04 – 90.9 nm. The physical  
22 parameters (i.e., slip length, surface tension, contact angle, and density) used in the simulation are  
23 listed in Table 2.

24 For each particle for which flow was observed, simulations were run using a half torus geometry,  
25 similar to the geometry observed in the experiments where flow was observed. The radius of the  
26 tube,  $R$ , in the half torus geometry and the radius of the hole,  $r$ , in the half torus geometry used in  
27 the simulations were based on the images recorded immediately after poking the particles with the  
28 needle. To determine viscosity for each particle, viscosity in the simulations was adjusted until  
29  $\tau_{\text{model, flow}}$  was within 1% of  $\tau_{\text{exp, flow}}$ .

30 In cases for which the particles cracked, simulations were run using a quarter-sphere model with  
31 one of the flat faces of the quarter sphere in contact with the substrate, similar to what was observed



1 in the experiments (Renbaum-Wolff et al., 2013a). The diameter used for the quarter sphere was  
2 20  $\mu\text{m}$ . In this case we determined a lower limit to the viscosity by adjusting the viscosity in the  
3 simulation until the sharp edge of the quarter sphere model moved by 0.5  $\mu\text{m}$  within 5 hr. A value  
4 of 0.5  $\mu\text{m}$  was used since this amount of movement could be observed in the optical microscope  
5 experiments.

6

### 7 **3 Results**

8 Shown in Fig. 3 are the mean bead speeds of individual SOM samples (toluene 1, 2, 3, and 4)  
9 measured at different RH values between 60 and 90% RH (see Sect. 2.1). As the RH decreased  
10 from 89.9 to 60.7%, the average bead speed decreased by a factor of 22 from  $9.20 \times 10^{-4}$  to  $4.24 \times$   
11  $10^{-7} \mu\text{m} \cdot \text{ms}^{-1}$ . Sample-to-sample variation was less than the uncertainty in the measurements and,  
12 within uncertainty, the results for 60 - 100  $\mu\text{g} \cdot \text{m}^{-3}$  concentration agreed with the results for 600 -  
13 1000  $\mu\text{g} \cdot \text{m}^{-3}$  concentration.

14 Figure 4 shows the result of  $\tau_{\text{exp, flow}}$  as a function of RH for the different samples (toluene 5, 6, 7,  
15 and 8). The  $\tau_{\text{exp, flow}}$  increased from  $\sim 1$  s to  $\sim 2000$  s as RH decreased from 50 to 30% RH. The  $\tau_{\text{exp,}}$   
16  $\tau_{\text{flow}}$  variation from sample to sample was less than the variation within individual toluene samples  
17 with mass concentrations over the range studied (600-1000 and 60-100  $\mu\text{g} \cdot \text{m}^{-3}$ ), as shown in Fig.  
18 4.

19 Shown in Fig. 5 are the viscosities as a function of RH for toluene-derived SOM particles  
20 determined from the bead-mobility experiments (Sect. 2.2) and the poke-flow experiments in  
21 conjunction with the fluid simulation (Sect. 2.3). For the bead-mobility experiments, the viscosities  
22 were determined by the mean of bead speeds between 60 and 90% RH. The  $y$ -error bars indicate  
23 the 95% prediction intervals from the calibration line (Song et al., 2015). The  $x$ -error bars represent  
24 the uncertainty in the RH measurements. The viscosity of the SOM increases from  $\sim 0.2$  to  $\sim 129$   
25 Pa·s as RH decreases from 89.9 to 60.7%. As shown in Fig. 5, difference between the results for  
26 the 600-1000 and 60-100  $\mu\text{g} \cdot \text{m}^{-3}$  samples are less than the uncertainties in the measurements.

27 Also shown in Fig. 5 are the calculated viscosities of the toluene-derived SOM for RH < 50% from  
28 the poke-flow experiments. The viscosity increases from approximately  $7.8 \times 10^3$  to  $6.3 \times 10^6$  Pa·s





1 as RH decreases from 47.3 to 30.5%. The uncertainty in the viscosity of approximately two orders  
2 of magnitude arises from the uncertainties in the physical parameters used in the simulations. For  
3  $RH < 20\%$ , restorative flow did not occur over  $\sim 5$  hrs resulting in a lower limit to the viscosity of  
4  $\sim 2 \times 10^8 \text{ Pa}\cdot\text{s}$ , similar to or greater than the viscosity of tar pitch ( $\sim 10^8 \text{ Pa}\cdot\text{s}$ , Koop et al. (2011)).

5

#### 6 **4 Discussion**

7 Bateman et al. (2015) previously estimated the viscosity of toluene-derived SOM from particle  
8 rebound experiments. From their measurements they estimated a viscosity of 100 to 1 Pa·s for  
9 RHs between 60 and 80% with SOM mass concentrations of 30 - 50  $\mu\text{g}\cdot\text{m}^{-3}$  (green box in Fig. 5)  
10 in good agreement with our measurements.

11 Li et al. (2015) previously estimated the diffusion coefficient of carboxylic acids within toluene-  
12 derived SOM from measurements of reactive uptake of  $\text{NH}_3$ . They estimated a diffusion  
13 coefficient  $10^{17.5 \pm 0.5} \text{ m}^2\cdot\text{s}^{-1}$  for RHs between 35 and 45% using SOM mass concentrations of 44 to  
14 125  $\mu\text{g}\cdot\text{m}^{-3}$ . If a hydrodynamic radius of 0.1 - 1.5 nm is assumed (Li et al., 2015), viscosity of  $1 \times$   
15  $10^4 - 2 \times 10^6 \text{ Pa}\cdot\text{s}$  is calculated using the Stokes-Einstein equation (blue box in Fig. 5), consistent  
16 with our measurements. The good agreement between the current results and the results from  
17 Bateman et al. and Li et al. suggests that the viscosity of the toluene-derived SOM is relatively  
18 insensitive to the particle mass concentrations at which the SOM is produced over the range of 30  
19 to 1000  $\mu\text{g}\cdot\text{m}^{-3}$ .

20 A liquid is defined as a material with a viscosity less than  $10^2 \text{ Pa}\cdot\text{s}$ ; a semisolid is defined as a  
21 material with a viscosity between  $10^2 \text{ Pa}\cdot\text{s}$  and  $10^{12} \text{ Pa}\cdot\text{s}$ ; and a solid is defined as a material with  
22 a viscosity greater than  $10^{12} \text{ Pa}\cdot\text{s}$  (Koop et al., 2011; Shiraiwa et al., 2011). As shown in Fig. 5,  
23 the viscosities of the SOM produced from toluene photo-oxidation correspond to liquid for  $RH >$   
24 60%, a semisolid for  $60\% < RH < 30\%$ , and a semisolid or a solid for  $RH < 20\%$ . Our results  
25 suggest a semisolid-to-liquid phase transition at an RH between 60 and 70%, in good agreement  
26 with Bateman et al. (2015) who suggested a semisolid-to-liquid phase transition of toluene-derived  
27 SOM particles in the range of 60 - 80% RH.



1 From the viscosities determined at  $295 \pm 1$  K and the Stokes-Einstein relationship (assuming a  
2 hydrodynamic radius of 0.4 nm for organic molecules within the toluene-derived SOM, Renbaum-  
3 Wolff et al., 2013a), we calculated the diffusion coefficients of large organic molecules,  $D_{org}$ ,  
4 within toluene-derived SOM (see secondary y-axis in Fig. 5).  $D_{org}$  ranges from  $\sim 3 \times 10^{-8}$  to  $\sim 2 \times$   
5  $10^{-15} \text{ cm}^2 \cdot \text{s}^{-1}$  for RH from 90 to 30%. It is lower than  $\sim 3 \times 10^{-17} \text{ cm}^2 \cdot \text{s}^{-1}$  for  $\text{RH} \leq 17\%$ . The Stokes-  
6 Einstein relation is not expected to predict with high accuracy the diffusion rates of small gas  
7 molecules such as OH, O<sub>3</sub>, NO<sub>x</sub>, NH<sub>3</sub>, and H<sub>2</sub>O (Koop et al., 2011; Shiraiwa et al., 2011). However,  
8 the Stokes-Einstein relationship should give reasonable estimations of diffusion rates for large  
9 organic molecules for conditions not close to the glass transition temperature of the matrix  
10 (Champion et al., 2000; Koop et al., 2011; Shiraiwa et al., 2011; Power et al., 2013). However, the  
11 relationship may be inaccurate near the glass transition RH (Champion et al., 2000; Shiraiwa et al.,  
12 2011; Power et al., 2013).

13 Using the diffusion coefficients ( $D_{org}$ ), the mixing time by diffusion,  $\tau_{mixing}$ , of large organic  
14 molecules within a 200 nm SOM particle was calculated with the following equation, where  $d$  is  
15 the particle diameter (Shiraiwa et al., 2011; Bones et al., 2012; Renbaum-Wolff et al., 2013a):

$$16 \quad \tau_{mixing} = \frac{d^2}{4\pi^2 D_{org}} \quad (\text{Eq.1})$$

17 Here we are using 200 nm to represent a typical accumulation mode atmospheric particle, Shiraiwa  
18 et al. (2011). The concentration of the diffusing molecules anywhere in the particles deviates by  
19 less than  $e^{-1}$  from the homogeneously well-mixed case at times longer than  $\tau_{mixing}$ . The  $\tau_{mixing}$  values  
20 calculated with this procedure are indicated in Fig. 5 (secondary y-axis). At an RH of 45% or  
21 higher, the mixing times are short, approaching less than or equal to 0.1 h. At 30% RH the mixing  
22 times are between 0.1 and 5 h. At  $\text{RH} \leq 17\%$  the mixing time is longer than  $\sim 100$  h.

23

## 24 **5 Atmospheric implications**

25 In the following, we use the mixing times calculated in the previous section to estimate the mixing  
26 times of large organic molecules in organic particulate matter over megacities. Several caveats  
27 should be kept in mind when applying the mixing times discussed earlier to particles over  
28 megacities. First, we are assuming that toluene-derived SOM is a good proxy for organic



1 particulate matter over megacities. Organic particulate matter over megacities are most likely more  
2 complicated and may include inorganic components. Second, the toluene-derived SOM was  
3 generated using relatively large mass concentrations of particles ( $60 - 1000 \mu\text{g}\cdot\text{m}^{-3}$ ). The good  
4 agreement between our results and the results from Bateman et al. (2015) and Li et al. (2015),  
5 which were carried out with a mass concentration of  $30 - 1000 \mu\text{g}\cdot\text{m}^{-3}$ , suggests that for toluene-  
6 derived SOM the viscosity is not strongly dependent on the mass concentration of organics used  
7 to generated the SOM, but additional studies are needed to confirm this. Third, as mentioned above,  
8 the Stokes-Einstein equation was used to estimate diffusion coefficients and hence mixing times,  
9 and this equation can underestimate diffusion coefficients close to the glass transition temperature.  
10 Despite these caveats, our estimates below should be a useful first-order approximation to the  
11 mixing times of large organics in organic particulate matter over megacities.

12 For this analysis we define megacity as a metropolitan area with a total population in excess of ten  
13 million people. Based on the Population Division Data Query (2014) of the United Nations  
14 (<http://esa.un.org/>), we selected the top 15 most populous cities (Tokyo, Delhi, Shanghai, Mexico  
15 City, São Paulo, Mumbai, Osaka, Beijing, New York, Cairo, Dhaka, Karachi, Buenos Aires,  
16 Kolkata, and Istanbul) which meet this criterion.

17 In order to determine  $\tau_{mixing}$  for organic particulate matter in megacities, information on the RH in  
18 the cities is needed. Fig. 6 gives information on RH and temperature in the 15 most populous  
19 megacities obtained from NOAA's National Climatic Data Center (NCDC) ([www.ncdc.noa.gov](http://www.ncdc.noa.gov)).  
20 The figure shows boxplots of average afternoon (3:00 – 5:00 local time) RH and temperature from  
21 these cities for the years from 2004 – 2014. The afternoon (3:00 – 5:00 local time) was chosen for  
22 this analysis since this is the time of day when RH is typically the lowest. In the figure, the boxes  
23 represent the median, 25<sup>th</sup> and 75<sup>th</sup> percentiles and the whiskers show the 10<sup>th</sup> and 90<sup>th</sup> percentiles.

24 In the Fig. 6, we indicate with green shading cases when the afternoon RH (at the 10<sup>th</sup> percentile  
25 level) does not go below 45% RH. The cases when the afternoon RH (at the 10<sup>th</sup> percentile level)  
26 does not go below 45 % RH are listed in Table 3 (second column). At 45% RH the mixing time  
27 within toluene-derived SOM is short (i.e., less than or equal to 0.1 h). Figure 6 (green shading)  
28 and Table 3 suggests that, if the organic particulate matter over megacities is similar to the toluene-  
29 derived SOM in this study, in Kolkata, Istanbul, Dhaka, Tokyo, Shanghai, and Mumbai, mixing



1 times during extended periods of the year will be very short, and homogeneously well-mixed  
2 particles can be assumed.

3 In the Fig. 6, we indicate with red shading cases where the afternoon RH (at the 10<sup>th</sup> percentile  
4 level) is 17% or lower. The cases when the afternoon RH (at the 10<sup>th</sup> percentile level) is 17 % or  
5 lower are listed in Table 3 (third column). As mentioned above, at this RH, the mixing time within  
6 toluene-derived SOM is long (> 100 h), based on the viscosity measurements and Stokes-Einstein  
7 calculations. Fig. 6 (red shading) and Table 3 (third column) suggests that if the organic particulate  
8 matter is similar to the toluene-derived SOM in this study, in Delhi, Beijing, Mexico City, Cairo,  
9 and Karachi, the particles may not be well-mixed in the afternoon (3:00 – 5:00 local time) during  
10 certain times of the year. If the breakdown to the Stokes-Einstein relationship is large at high  
11 viscosities the number of cases classified as having particles not well-mixed may be less than  
12 indicated. Hence, the number of cases classified as having particles not well-mixed based on the  
13 viscosity data presented here and the Stokes-Einstein relationship should be considered as an upper  
14 limit.

15 Another caveat to the discussion above is the effect of temperature on viscosity. The conclusions  
16 reached above were based on viscosity measurements carried out at  $295 \pm 1$  K, while the  
17 temperatures shown in Fig. 6 ranges from roughly 0 °C to 40 °C. Viscosity is known to decrease  
18 as the temperature increases, but the effect of temperature on the viscosity of SOM has not been  
19 quantified. Studies that quantify the effect of temperature on the viscosity of SOM are needed for  
20 more accurate predictions of the mixing times in organic particulate matter over megacities.

21 Kleinman et al., (2009) studied the time evolution of aerosol size distributions and number  
22 concentrations of ambient particulate matter over the Mexico City plateau during the MILAGRO  
23 (Megacity Initiative: Local And Global Research Observations) field campaign conducted in  
24 March 2006. The particulate matter over Mexico City was primarily organic and as photochemical  
25 aging occurred, Kleinman and colleagues observed an increase in accumulation-mode volume due  
26 to an increase in the accumulation mode particles, not because of an increase in the average size  
27 of the accumulation mode. The condensing organic vapors from photooxidation of toluene and  
28 other anthropogenic VOCs over Mexico City are expected to be semivolatile (Shrivastava et al.,  
29 2013). However, Kleinman et al. showed that the observed evolution of aerosol size distribution  
30 was not consistent with a volume growth mechanism in which the semivolatile organic vapors are



1 expected to readily diffuse within the accumulation mode substrate. This could indicate that the  
2 accumulation mode particles over Mexico City were highly viscous and did not reach equilibrium  
3 with large gas-phase organic molecules during the observation period. This observation is  
4 consistent with our experimental results that toluene-derived SOM is highly viscous at  $RH < 20\%$   
5 and Fig. 6, which shows that the median  $RH$  in Mexico City often falls below 20% in March.  
6 However, it should be noted that the particulate matter over Mexico City is likely more chemically  
7 complex than the SOM used in this study.

8

## 9 **6 Conclusions**

10 We investigated the  $RH$ -dependent viscosities at room temperature of SOM particles produced  
11 from toluene photo-oxidation with the mass concentration of  $60 - 1000 \mu\text{g}\cdot\text{m}^{-3}$ . A bead-mobility  
12 technique showed the viscosities of the toluene-derived SOM increased from  $\sim 0.2$  to  $\sim 129 \text{ Pa}\cdot\text{s}$  as  
13  $RH$  decrease from 89.9 to 60.7%. This indicates that the toluene-derived SOM particles are a liquid  
14 at  $RH > 60\%$ . The  $RH$  range for liquid-to-semisolid is in good agreement with Bateman et al.  
15 (2015) who showed the liquid-to-semisolid phase transition of these particles in the range of 60-  
16 80%  $RH$ . A poke-flow technique combined with fluid simulations showed the viscosities increased  
17 from approximately  $7.8 \times 10^3$  to  $6.3 \times 10^6 \text{ Pa}\cdot\text{s}$  as  $RH$  decreases from 47.3 to 30.5%. For  $RH \leq$   
18 17%, the viscosities of the SOM were greater than or equal to  $\sim 2 \times 10^8 \text{ Pa}\cdot\text{s}$ , similar to or greater  
19 than the viscosity of tar pitch. This suggests that the toluene-derived SOM particles are a semisolid  
20 at  $20 < RH \leq 60\%$ , and a semisolid or a solid at  $RH \leq 17\%$ . Using the viscosity data and the Stokes-  
21 Einstein equation, the diffusion coefficients of large gas-phase organic molecules within the  
22 toluene-derived SOM particles were calculated to be  $\sim 3 \times 10^{-8}$  to  $\sim 2 \times 10^{-15} \text{ cm}^2 \text{ s}^{-1}$  for  $RH$ s from  
23 89.9 to 30.5%, and is lower than  $\sim 3 \times 10^{-17} \text{ cm}^2 \text{ s}^{-1}$  for  $RH \leq 17\%$ . Mixing time by diffusion of  
24 large organic molecules within 200 nm toluene-derived SOM particles was calculated to be less  
25 than 0.1 h at  $RH < 47.3\%$ , 0.5 - 5 h at 30.5%  $RH$ , and greater than  $\sim 100$  h at  $RH \leq 17\%$ .

26 To apply the results of the viscosities, diffusion coefficients, and mixing time of the toluene-  
27 derived SOM, we selected the top 15 most populous megacities. Based on the  $RH$  in the cities, and  
28 if the organic particulate matter in megacities is similar to the toluene-derived SOM in this study,  
29 in cities such as Kolkata, Istanbul, Dhaka, Tokyo, Shanghai, and Mumbai, mixing times during



1 extended periods of the year will be very short and homogeneously well-mixed particles can be  
2 assumed. On the other hand, for certain times of the year in Delhi, Beijing, Mexico City, Cairo,  
3 and Karachi, mixing times of large organic molecules in organic particulate matter may be long ( $\geq$   
4 100 hr), and the particles may not be well mixed in the afternoon (3:00 – 5:00 local time) during  
5 certain times of the year. These results are summarized in Fig. 7.

6

## 7 **Acknowledgments**

8 This work was supported by the Natural Sciences and Engineering Research Council of Canada.  
9 Support from the USA National Science Foundation, the Atmospheric Science Research (ASR)  
10 Program of the USA Department of Energy, and research funds for newly appointed professors of  
11 Chonbuk National University in 2015 is also acknowledged.

12

## 13 **References**

14 Abramson, E., Imre, D., Beranek, J., Wilson, J., and Zelenyuk, A.: Experimental determination of  
15 chemical diffusion within secondary organic aerosol particles, *Phys. Chem. Chem. Phys.*, 15,  
16 2983-2991, Doi 10.1039/C2cp44013j, 2013.

17 Adamson, A. W., and Gast A. P.: *Physical chemistry of surfaces*, 6<sup>th</sup> edition, ISBN: 978-0-471-  
18 14873-9, 1997.

19 Bateman, A. P., Bertram, A. K., and Martin, S. T.: Hygroscopic influence on the semisolid-to-  
20 liquid transition of secondary organic materials, *J. Phys. Chem. A.*, 119 (19), pp 4386–4395 ,  
21 Doi:10.1021/jp508521c, 2015.

22 Baudry, J., Charlaix, E., Tonck, A., and Mazuyer, D.: Experimental evidence for a large slip effect  
23 at a nonwetting fluid-solid interface, *Langmuir*, 17, 5232-5236, Doi 10.1021/La0009994, 2001.

24 Bertram, A. K., Martin, S. T., Hanna, S. J., Smith, M. L., Bodsworth, A., Chen, Q., Kuwata, M.,  
25 Liu, A., You, Y., and Zorn, S. R.: Predicting the relative humidities of liquid-liquid phase  
26 separation, efflorescence, and deliquescence of mixed particles of ammonium sulfate, organic



- 1 material, and water using the organic-to-sulfate mass ratio of the particle and the oxygen-to-carbon  
2 elemental ratio of the organic component, Atmos. Chem. Phys., 11, 10995-11006, Doi  
3 10.5194/acp-11-10995-2011, 2011.
- 4 Bodsworth, A., Zobrist, B., and Bertram, A. K.: Inhibition of efflorescence in mixed organic-  
5 inorganic particles at temperatures less than 250K, Phys. Chem. Chem. Phys., 12, 15144-15144,  
6 2010.
- 7 Bones, D. L., Reid, J. P., Lienhard, D. M., and Krieger, U. K.: Comparing the mechanism of  
8 water condensation and evaporation in glassy aerosol, P. Natl. Acad. Sci. USA, 109, 11613–11618,  
9 doi:10.1073/pnas.1200691109, 2012.
- 10 Cappa, C. D., and Wilson, K. R.: Evolution of organic aerosol mass spectra upon heating:  
11 implications for OA phase and partitioning behavior, Atmos. Chem. Phys., 11, 1895-1911, Doi  
12 10.5194/acp-11-1895-2011, 2011.
- 13 Champion, D., Le Meste, M., and Simatos, D.: Towards an improved understanding of glass  
14 transition and relaxations in foods: molecular mobility in the glass transition range, Trends Food  
15 Sci. Tech., 11, 41-55, Doi 10.1016/S0924-2244(00)00047-9, 2000.
- 16 Cheng, J. T., and Giordano, N.: Fluid flow through nanometer-scale channels, Phys. Rev.E, 65,  
17 Artn 031206, Doi 10.1103/Physreve.65.031206, 2002.
- 18 Churaev, N. V., Sobolev, V. D., and Somov, A. N.: Slippage of liquids over lyophobic solid-  
19 surfaces, J. Colloid Interf. Sci., 97, 574-581, Doi 10.1016/0021-9797(84)90330-8, 1984.
- 20 Craig, V. S. J., Neto, C., and Williams, D. R. M.: Shear-dependent boundary slip in an aqueous  
21 Newtonian liquid, Phys. Rev. Lett, 87, Artn 054504, Doi 10.1103/Physrevlett.87.054504, 2001.
- 22 Decesari, S., Fuzzi, S., Facchini, M. C., Mircea, M., Emblico, L., Cavalli, F., Maenhaut, W., Chi,  
23 X., Schkolnik, G., Falkovich, A., Rudich, Y., Claeys, M., Pashynska, V., Vas, G., Kourtchev, I.,  
24 Vermeylen, R., Hoffer, A., Andreae, M. O., Tagliavini, E., Moretti, F., and Artaxo, P.:  
25 Characterization of the organic composition of aerosols from Rondonia, Brazil, during the LBA-  
26 SMOCC 2002 experiment and its representation through model compounds, Atmos. Chem. Phys.,  
27 6, 375-402, 2006.



- 1 Engelhart, G. J., Asa-Awuku, A., Nenes, A., and Pandis, S. N.: CCN activity and droplet growth  
2 kinetics of fresh and aged monoterpene secondary organic aerosol, *Atmos. Chem. Phys.*, 8, 3937-  
3 3949, 2008.
- 4 Grayson, J. W., Song, M., Sellier, M., and Bertram, A. K.: Validation of the poke-flow technique  
5 combined with simulations of fluid flow for determining viscosities in samples with small volumes  
6 and high viscosities, *Atmos. Meas. Tech.*, 8, 2463-2472, 2015a.
- 7 Grayson, J. W., Zhang, Y., Mutzel, A., Renbaum-Wolff, L., Böge, O., Kamal, S., Herrmann, H.,  
8 Martin, S. T., and Bertram, A. K.: Effect of varying experimental conditions on the viscosity of  $\alpha$ -  
9 pinene derived secondary organic material, *Atmos. Chem. Phys. Discuss.*, 15, 32967-33002,  
10 doi:10.5194/acpd-15-32967-2015, 2015b.
- 11 Hallquist, M., Wenger, J. C., Baltensperger, U., Rudich, Y., Simpson, D., Claeys, M., Dommen,  
12 J., Donahue, N. M., George, C., Goldstein, A. H., Hamilton, J. F., Herrmann, H., Hoffmann, T.,  
13 Iinuma, Y., Jang, M., Jenkin, M. E., Jimenez, J. L., Kiendler-Scharr, A., Maenhaut, W., McFiggans,  
14 G., Mentel, T. F., Monod, A., Prevot, A. S. H., Seinfeld, J. H., Surratt, J. D., Szmigielski, R., and  
15 Wildt, J.: The formation, properties and impact of secondary organic aerosol: current and emerging  
16 issues, *Atmos. Chem. Phys.*, 9, 5155-5236, 2009.
- 17 Hildebrandt, L., Donahue, N. M., and Pandis, S. N.: High formation of secondary organic aerosol  
18 from the photo-oxidation of toluene, *Atmos. Chem. Phys.*, 9, 2973–2986, doi:10.5194/acp-9-2973-  
19 2009, 2009.
- 20 Houle, F. A., Hinsberg, W. D., and Wilson, K. R.: Oxidation of a model alkane aerosol by OH  
21 radical: the emergent nature of reactive uptake, *Phys. Chem. Chem. Phys.*, 17, 4412-4423, 2015.
- 22 Jimenez, J. L., Canagaratna, M. R., Donahue, N. M., Prevot, A. S. H., Zhang, Q., Kroll, J. H.,  
23 DeCarlo, P. F., Allan, J. D., Coe, H., Ng, N. L., Aiken, A. C., Docherty, K. S., Ulbrich, I. M.,  
24 Grieshop, A. P., Robinson, A. L., Duplissy, J., Smith, J. D., Wilson, K. R., Lanz, V. A., Hueglin,  
25 C., Sun, Y. L., Tian, J., Laaksonen, A., Raatikainen, T., Rautiainen, J., Vaattovaara, P., Ehn, M.,  
26 Kulmala, M., Tomlinson, J. M., Collins, D. R., Cubison, M. J., Dunlea, E. J., Huffman, J. A.,  
27 Onasch, T. B., Alfarra, M. R., Williams, P. I., Bower, K., Kondo, Y., Schneider, J., Drewnick, F.,  
28 Borrmann, S., Weimer, S., Demerjian, K., Salcedo, D., Cottrell, L., Griffin, R., Takami, A.,





- 1 Miyoshi, T., Hatakeyama, S., Shimono, A., Sun, J. Y., Zhang, Y. M., Dzepina, K., Kimmel, J. R.,  
2 Sueper, D., Jayne, J. T., Herndon, S. C., Trimborn, A. M., Williams, L. R., Wood, E. C.,  
3 Middlebrook, A. M., Kolb, C. E., Baltensperger, U., and Worsnop, D. R.: Evolution of organic  
4 aerosols in the atmosphere, *Science*, 326, 1525-1529, Doi 10.1126/science.1180353, 2009.
- 5 Jin, S., Huang, P., Park, J., Yoo, J. Y., and Breuer, K. S.: Near-surface velocimetry using  
6 evanescent wave illumination, *Exp. Fluids*, 37, 825-833, Doi 10.1007/s00348-004-0870-7, 2004.
- 7 Joly, L., Ybert, C., and Bocquet, L.: Probing the nanohydrodynamics at liquid-solid interfaces  
8 using thermal motion, *Phys. Rev. Lett.*, 96, Artn 046101, Doi 10.1103/Physrevlett.96.046101, 2006.
- 9 Joseph, P., and Tabeling, P.: Direct measurement of the apparent slip length, *Phys. Rev. E*, 71,  
10 Artn 035303, Doi 10.1103/Physreve.71.035303, 2005.
- 11 Kang, E., Root, M. J., Toohey, D. W., and Brune, W. H.: Introducing the concept of Potential  
12 Aerosol Mass (PAM), *Atmos. Chem. Phys.*, 7, 5727–5744, Doi:10.5194/acp-7-5727-2007, 2007.
- 13 Kidd, C., Perraud, V., Wingen, L. M., and Finlayson-Pitts, B. J.: Integrating phase and composition  
14 of secondary organic aerosol from the ozonolysis of alpha-pinene, *P. Natl. Acad. Sci. USA*, 111,  
15 7552-7557, Doi 10.1073/pnas.1322558111, 2014.
- 16 Kleinman, L. I., Springston, S. R., Wang, J., Daum, P. H., Lee, Y. N., Nunnermacker, L. J., Senum,  
17 G. I., Weinstein-Lloyd, J., Alexander, M. L., Hubbe, J., Ortega, J., Zaveri, R. A., Canagaratna, M.  
18 R., and Jayne, J.: The time evolution of aerosol size distribution over the Mexico City plateau,  
19 *Atmos. Chem. Phys.*, 9, 4261-4278, 2009.
- 20 Knopf, D. A.: Thermodynamic properties and nucleation processes of upper tropospheric and  
21 lower stratospheric aerosol particles, Diss. ETH No. 15103, Zurich, Switzerland, 2003.
- 22 Koop, T., Bookhold, J., Shiraiwa, M., and Poschl, U.: Glass transition and phase state of organic  
23 compounds: dependency on molecular properties and implications for secondary organic aerosols  
24 in the atmosphere, *Phys. Chem. Chem. Phys.*, 13, 19238-19255, Doi 10.1039/C1cp22617g, 2011.
- 25 Kuwata, M., and Martin, S. T.: Phase of atmospheric secondary organic material affects its  
26 reactivity, *P. Natl. Acad. Sci. USA*, 109, 17354-17359, 10.1073/pnas.1209071109, 2012.



- 1   Ladino, L. A., Zhou, S., Yakobi-Hancock, J. D., Aljawhary, D., and Abbatt, J. P. D.: Factors  
2   controlling the ice nucleating abilities of alpha-pinene SOA particles, *J. Geophys. Res-Atmos.*,  
3   119, 9041-9051, 2014.
- 4   Lambe, A. T., Ahern, A. T., Williams, L. R., Slowik, J. G., Wong, J. P. S., Abbatt, J. P. D., Brune,  
5   W. H., Ng, N. L., Wright, J. P., Croasdale, D. R., Worsnop, D. R., Davidovits, P., and Onasch, T.  
6   B.: Characterization of aerosol photooxidation flow reactors: het-erogeneous oxidation, secondary  
7   organic aerosol formation and cloud condensation nuclei activity measurements, *Atmos. Meas.*  
8   *Tech.*, 4, 445–461, doi:10.5194/amt-4-445-2011, 2011.
- 9   Li, Y. J., Liu, P. F. Gong, Z. Wang, Y., Bateman, A. P., Bergoend, C., Bertram, A. K., and Martin,  
10   S. T.: Chemical reactivity and liquid/non-liquid states of secondary organic material, *Environ. Sci.*  
11   *Technol.*, 49 (22), pp 13264–13274, Doi: 10.1021/acs.est.5b03392, 2015
- 12   Li, L., Mo, J. W., and Li, Z. L.: Flow and slip transition in nanochannels, *Phys. Rev. E*, 90, Artn  
13   033003, Doi 10.1103/Physreve.90.033003, 2014.
- 14   Liu, P. F., Zhang, Y., and Martin, S. T.: Complex refractive indices of thin films of secondary  
15   organic materials by spectroscopic ellipsometry from 220 to 1200 nm, *Environ. Sci. Technol.*, 47,  
16   13594-13601, Doi 10.1021/Es403411e, 2013.
- 17   Martin, S. T.: Phase transitions of aqueous atmospheric particles, *Chem. Rev.*, 100, 3403-3453,  
18   doi 10.1021/Cr990034t, 2000.
- 19   Murray, B. J.: Inhibition of ice crystallisation in highly viscous aqueous organic acid droplets,  
20   *Atmos. Chem. Phys.*, 8, 5423-5433, 2008.
- 21   Murray, B. J., and Bertram, A. K.: Inhibition of solute crystallisation in aqueous  $\text{H}^+$ - $\text{NH}_4^+$ - $\text{SO}_4^{2-}$ -  
22    $\text{H}_2\text{O}$  droplets, *Phys. Chem. Chem. Phys.*, 10, 3287-3301, 2008.
- 23   Murray, B. J., Haddrell, A. E., Peppe, S., Davies, J. F., Reid, J. P., O'Sullivan, D., Price, H. C.,  
24   Kumar, R., Saunders, R. W., Plane, J. M. C., Umo, N. S., and Wilson, T. W.: Glass formation and  
25   unusual hygroscopic growth of iodine acid solution droplets with relevance for iodine mediated  
26   particle formation in the marine boundary layer, *Atmos. Chem. Phys.*, 12, 8575-8587, DOI  
27   10.5194/acp-12-8575-2012, 2012.



- 1 Murray, B. J., Wilson, T. W., Dobbie, S., Cui, Z. Q., Al-Jumur, S. M. R. K., Mohler, O., Schnaiter,  
2 M., Wagner, R., Benz, S., Niemand, M., Saathoff, H., Ebert, V., Wagner, S., and Karcher, B.:  
3 Heterogeneous nucleation of ice particles on glassy aerosols under cirrus conditions, *Nat. Geosci.*,  
4 3, 233-237, Doi 10.1038/Ngeo817, 2010.
- 5 Ng, N. L., Kroll, J. H., Chan, A. W. H., Chhabra, P. S., Flagan, R. C., and Seinfeld, J. H.: Secondary  
6 organic aerosol formation from m-xylene, toluene, and benzene, *Atmos. Chem. Phys.*, 7, 3909-  
7 3922, 2007.
- 8 Pajunoja, A., Malila, J., Hao, L. Q., Joutsensaari, J., Lehtinen, K. E. J., and Virtanen, A.:  
9 Estimating the Viscosity Range of SOA Particles Based on Their Coalescence Time, *Aerosol Sci.*  
10 *Tech.*, 48, I-Iv, Doi 10.1080/02786826.2013.870325, 2014.
- 11 Pandis, S. N., Harley, R. A., Cass, G. R., and Seinfeld, J. H.: Secondary organic aerosol formation  
12 and transport, *Atmos. Environ. a-Gen.*, 26, 2269-2282, 1992.
- 13 Pant, A., Parsons, M. T., and Bertram, A. K.: Crystallization of aqueous ammonium sulfate  
14 particles internally mixed with soot and kaolinite: Crystallization relative humidities and  
15 nucleation rates, *J. Phys. Chem. A*, 110, 8701-8709, Doi 10.1021/Jp060985s, 2006.
- 16 Perraud, V., Bruns, E. A., Ezell, M. J., Johnson, S. N., Yu, Y., Alexander, M. L., Zelenyuk, A.,  
17 Imre, D., Chang, W. L., Dabdub, D., Pankow, J. F., and Finlayson-Pitts, B. J.: Nonequilibrium  
18 atmospheric secondary organic aerosol formation and growth, *P. Natl. Acad. Sci. USA*, 109, 2836-  
19 2841, Doi 10.1073/pnas.1119909109, 2012.
- 20 Pöschl, U., Martin, S. T., Sinha, B., Chen, Q., Gunthe, S. S., Huffman, J. A., Borrmann, S., Farmer,  
21 D. K., Garland, R. M., Helas, G., Jimenez, J. L., King, S. M., Manzi, A., Mikhailov, E., Pauliquevis,  
22 T., Petters, M. D., Prenni, A. J., Roldin, P., Rose, D., Schneider, J., Su, H., Zorn, S. R., Artaxo, P.,  
23 and Andreae, M. O.: Rainforest aerosols as biogenic nuclei of clouds and precipitation in the  
24 Amazon, *Science*, 329, 1513-1516, Doi 10.1126/science.1191056, 2010.
- 25 Power, R. M., Simpson, S. H., Reid, J. P., and Hudson, A. J.: The transition from liquid to solid-  
26 like behaviour in ultrahigh viscosity aerosol particles, *Chem. Sci.*, 4, 2597-2604, Doi  
27 10.1039/C3sc50682g, 2013.



- 1 Prenni, A. J., Petters, M. D., Kreidenweis, S. M., Heald, C. L., Martin, S. T., Artaxo, P., Garland,  
2 R. M., Wollny, A. G., and Poschl, U.: Relative roles of biogenic emissions and Saharan dust as ice  
3 nuclei in the Amazon basin, *Nat. Geosci.*, 2, 401-404, doi 10.1038/Ngeo517, 2009.
- 4 Price, H. C., Mattsson, J., Zhang, Y., Bertram, A. K., Davies, J. F., Grayson, J. W., Martin, S. T.,  
5 O'Sullivan, D., Reid, J. P., Rickards, A. M. J., and Murray, B. J.: Water diffusion in  
6 atmospherically relevant alpha-pinene secondary organic material, *Chem. Sci.*, 6, 4876-4883, 2015.
- 7 Reist, P.: *Aerosol Science and Technology*, McGraw-Hill Professional, New York, NY, USA, 2  
8 Edn., 1992.
- 9 Renbaum-Wolff, L., Grayson, J. W., Bateman, A. P., Kuwata, M., Sellier, M., Murray, B. J.,  
10 Shilling, J. E., Martin, S. T., and Bertram, A. K.: Viscosity of alpha-pinene secondary organic  
11 material and implications for particle growth and reactivity, *P. Natl. Acad. Sci. USA*, 110, 8014-  
12 8019, Doi 10.1073/pnas.1219548110, 2013.
- 13 Renbaum-Wolff, L., Grayson, J. W., and Bertram, A. K.: Technical Note: New methodology for  
14 measuring viscosities in small volumes characteristic of environmental chamber particle samples,  
15 *Atmos. Chem. Phys.*, 13, 791-802, Doi 10.5194/acp-13-791-2013, 2013.
- 16 Renbaum-Wolff, L., Song, M., Marcolli, C., Zhang, Y., Liu, P. F., Grayson J. W., Geiger, F. M.,  
17 Martin, S. T., and Bertram, A. K.: Observations and implications of liquid-liquid phase separation  
18 at high relative humidities in secondary organic material produced by  $\alpha$ -pinene ozonolysis without  
19 inorganic salts, *Atmos. Chem. Phys.*, Submitted, 2015.
- 20 Riipinen, I., Pierce, J. R., Yli-Juuti, T., Nieminen, T., Hakkinen, S., Ehn, M., Junninen, H.,  
21 Lehtipalo, K., Petaja, T., Slowik, J., Chang, R., Shantz, N. C., Abbatt, J., Leaitch, W. R., Kerminen,  
22 V. M., Worsnop, D. R., Pandis, S. N., Donahue, N. M., and Kulmala, M.: Organic condensation:  
23 a vital link connecting aerosol formation to cloud condensation nuclei (CCN) concentrations,  
24 *Atmos. Chem. Phys.*, 11, 3865-3878, Doi 10.5194/acp-11-3865-2011, 2011.
- 25 Robinson, E. S., Saleh, R., and Donahue, N. M.: Organic aerosol mixing observed by single-  
26 particle mass spectrometry, *J. Phys. Chem. A*, 117, 13935-13945, Doi 10.1021/Jp405789t, 2013.
- 27 Saukko, E., Lambe, A. T., Massoli, P., Koop, T., Wright, J. P., Croasdale, D. R., Pedernera, D. A.,  
28 Onasch, T. B., Laaksonen, A., Davidovits, P., Worsnop, D. R., and Virtanen, A.: Humidity-



- 1 dependent phase state of SOA particles from biogenic and anthropogenic precursors, Atmos. Chem.  
2 Phys., 12, 7517-7529, Doi 10.5194/acp-12-7517-2012, 2012.
- 3 Schill, G. P., De Haan, D. O., and Tolbert, M. A.: Heterogeneous ice nucleation on simulated  
4 secondary organic aerosol, Environ. Sci. Technol., 48, 1675-1682, 2014.
- 5 Schnell, E.: Slippage of Water over Nonwetable Surfaces, J. Appl. Phys., 27, 1149-1152, Doi  
6 10.1063/1.1722220, 1956.
- 7 Shiraiwa, M., Ammann, M., Koop, T., and Poschl, U.: Gas uptake and chemical aging of semisolid  
8 organic aerosol particles, P. Natl. Acad. Sci. USA, 108, 11003-11008, Doi  
9 10.1073/pnas.1103045108, 2011.
- 10 Shiraiwa, M., and Seinfeld, J. H.: Equilibration timescale of atmospheric secondary organic  
11 aerosol partitioning, Geophys. Res. Lett., 39, Artn L24801, Doi 10.1029/2012gl054008, 2012.
- 12 Shrivastava, M., Zelenyuk, A., Imre, D., Easter, R., Beranek, J., Zaveri, R. A., and Fast, J.:  
13 Implications of low volatility SOA and gas-phase fragmentation reactions on SOA loadings and  
14 their spatial and temporal evolution in the atmosphere, J. Geophys. Res-Atmos., 118, 3328-3342,  
15 2013.
- 16 Song, M., Liu, P. F., Hanna, S. J., Li, Y. J., Martin, S. T., and Bertram, A. K.: Relative humidity-  
17 dependent viscosities of isoprene-derived secondary organic material and atmospheric  
18 implications for isoprene-dominant forests, Atmos. Chem. Phys., 15, 5145-5159, 2015.
- 19 Song, M., Marcolli, C., Krieger, U. K., Zuend, A., and Peter, T.: Liquid-liquid phase separation  
20 and morphology of internally mixed dicarboxylic acids/ammonium sulfate/water particles, Atmos.  
21 Chem. Phys., 12, 2691-2712, Doi 10.5194/acp-12-2691-2012, 2012.
- 22 Song, M. J., Marcolli, C., Krieger, U. K., Lienhard, D. M., and Peter, T.: Morphologies of mixed  
23 organic/inorganic/aqueous aerosol droplets, Faraday Discuss., 165, 289-316, Doi  
24 10.1039/C3fd00049d, 2013.
- 25 Steimer, S. S., Lampimaki, M., Coz, E., Grzanic, G., and Ammann, M.: The influence of physical  
26 state on shikimic acid ozonolysis: a case for in situ microspectroscopy, Atmos. Chem. Phys., 14,  
27 10761-10772, 2014.



- 1 Virtanen, A., Joutsensaari, J., Koop, T., Kannosto, J., Yli-Pirila, P., Leskinen, J., Makela, J. M.,  
2 Holopainen, J. K., Poschl, U., Kulmala, M., Worsnop, D. R., and Laaksonen, A.: An amorphous  
3 solid state of biogenic secondary organic aerosol particles, *Nature*, 467, 824-827,  
4 10.1038/nature09455, 2010.
- 5 Wang, B. B., Lambe, A. T., Massoli, P., Onasch, T. B., Davidovits, P., Worsnop, D. R., and Knopf,  
6 D. A.: The deposition ice nucleation and immersion freezing potential of amorphous secondary  
7 organic aerosol: Pathways for ice and mixed-phase cloud formation, *J. Geophys. Res-Atmos.*, 117,  
8 Artn D16209, Doi 10.1029/2012jd018063, 2012.
- 9 Watanabe, K., Yanuar, and Udagawa, H.: Drag reduction of Newtonian fluid in a circular pipe  
10 with a highly water-repellent wall, *J. Fluid Mech.*, 381, 225-238, Doi  
11 10.1017/S0022112098003747, 1999.
- 12 Wilson, T. W., Murray, B. J., Wagner, R., Mohler, O., Saathoff, H., Schnaiter, M., Skrotzki, J.,  
13 Price, H. C., Malkin, T. L., Dobbie, S., and Al-Jumur, S. M. R. K.: Glassy aerosols with a range  
14 of compositions nucleate ice heterogeneously at cirrus temperatures, *Atmos. Chem. Phys.*, 12,  
15 8611-8632, 2012.
- 16 Zaveri, R. A., Easter, R. C., Shilling, J. E., and Seinfeld, J. H.: Modeling kinetic partitioning of  
17 secondary organic aerosol and size distribution dynamics: representing effects of volatility, phase  
18 state, and particle-phase reaction, *Atmos. Chem. Phys.*, 14, 5153-5181, Doi 10.5194/acp-14-5153-  
19 2014, 2014.
- 20 Zelenyuk, A., Imre, D., Beranek, J., Abramson, E., Wilson, J., and Shrivastava, M.: Synergy  
21 between secondary organic aerosols and long-range transport of polycyclic aromatic hydrocarbons,  
22 *Environ. Sci. Technol.*, 46, 12459-12466, Doi 10.1021/Es302743z, 2012.
- 23 Zhang, Q., Jimenez, J. L., Canagaratna, M. R., Allan, J. D., Coe, H., Ulbrich, I., Alfarra, M. R.,  
24 Takami, A., Middlebrook, A. M., Sun, Y. L., Dzepina, K., Dunlea, E., Docherty, K., DeCarlo, P.  
25 F., Salcedo, D., Onasch, T., Jayne, J. T., Miyoshi, T., Shimonono, A., Hatakeyama, S., Takegawa,  
26 N., Kondo, Y., Schneider, J., Drewnick, F., Borrmann, S., Weimer, S., Demerjian, K., Williams,  
27 P., Bower, K., Bahreini, R., Cottrell, L., Griffin, R. J., Rautiainen, J., Sun, J. Y., Zhang, Y. M., and  
28 Worsnop, D. R.: Ubiquity and dominance of oxygenated species in organic aerosols in



1 anthropogenically-influenced Northern Hemisphere midlatitudes, *Geophys. Res. Lett.*, 34, -, Art  
2 L13801, Doi 10.1029/2007gl029979, 2007.

3 Zhou, S. M., Shiraiwa, M., McWhinney, R. D., Poschl, U., and Abbatt, J. P. D.: Kinetic limitations  
4 in gas-particle reactions arising from slow diffusion in secondary organic aerosol, *Faraday*  
5 *Discuss.*, 165, 391-406, Doi 10.1039/C3fd00030c, 2013.

6 Zhu, L. W., Neto, C., and Attard, P.: Reliable measurements of interfacial slip by colloid probe  
7 atomic force microscopy. III. shear-rate-dependent slip, *Langmuir*, 28, 3465-3473, Doi  
8 10.1021/La204566h, 2012.

9

10

11



- 1 Table 1. Experimental conditions for production and collection of toluene-derived SOM particles  
2 using the oxidation flow reactor. Particles were collected onto hydrophobic substrates using an  
3 electrostatic precipitator or a single stage impactor.

SOM sample name	Toluene conc. (ppm)	Ozone conc. (ppm)	SOM mass conc. during production ( $\mu\text{g m}^{-3}$ )	OFR flow rate ( $\text{L m}^{-1}$ )	Collection time (hr)	Collection method
For bead-mobility experiments						
Toluene 1	$1.0 \pm 0.1$	$30 \pm 3$	600-1000	$7.0 \pm 0.5$	48	Electrostatic precipitator
Toluene 2	$1.0 \pm 0.1$	$30 \pm 3$	600-1000	$7.0 \pm 0.5$	48	Electrostatic precipitator
Toluene 3	$0.1 \pm 0.01$	$30 \pm 3$	60-100	$7.0 \pm 0.5$	12	Impactor
Toluene 4	$0.1 \pm 0.01$	$30 \pm 3$	60-100	$7.0 \pm 0.5$	19	Impactor
For poke-flow experiments						
Toluene 5	$1.0 \pm 0.1$	$30 \pm 3$	600-1000	$7.0 \pm 0.5$	96	Electrostatic precipitator
Toluene 6	$1.0 \pm 0.1$	$30 \pm 3$	600-1000	$7.0 \pm 0.5$	96	Electrostatic precipitator
Toluene 7	$0.1 \pm 0.01$	$30 \pm 3$	60-100	$7.0 \pm 0.5$	12.5	Impactor
Toluene 8	$0.1 \pm 0.01$	$30 \pm 3$	60-100	$7.0 \pm 0.5$	16	Impactor

4

5





- 1 Table 2. Physical parameters used to simulate material flow in the poke-flow experiments.  $R$  and  
 2  $r$  indicate the radius of a tube and the radius of an inner hole, respectively.

	Slip length (nm)	Surface tension (mN m <sup>-1</sup> )	Density (g cm <sup>-3</sup> )	Contact angle (°)
Values used to calculate lower limit	5 <sup>a</sup>	28 <sup>b</sup>	1.4 <sup>c</sup>	80 (if $r < 2R$ ), 100 (if $r > 2R$ )
Values used to calculate upper limit	10000 <sup>a</sup>	75 <sup>d</sup>	1.4 <sup>c</sup>	80 (if $r < 2R$ ), 100 (if $r > 2R$ )

3 <sup>a</sup>The range of slip length, which is the interactions between fluids and solid surfaces, is based on  
 4 literature data (Schnell, 1956; Churaev et al., 1984; Watanabe et al., 1999; Baudry et al., 2001;  
 5 Craig et al., 2001; Tretheway and Meinhart, 2002; Cheng and Giordano, 2002; Jin et al., 2004;  
 6 Joseph and Tabeling, 2005; Neto et al., 2005; Choi and Kim et al., 2006; Joly et al., 2006; Zhu et  
 7 al., 2012; Li et al., 2014).

8 <sup>b</sup>The lower limits of the surface tension of toluene-derived SOM were determined as 28 mN m<sup>-1</sup>,  
 9 the surface tension of liquid toluene at 293 K (Adamson and Gast, 1997).

10 <sup>c</sup>Ng et al., 2007

11 <sup>d</sup>The upper limits of the surface tension of toluene-derived SOM were determined as 75 mN m<sup>-1</sup>,  
 12 the surface tension of pure water at 293 K (Engelhart et al., 2008).

13 <sup>e</sup>Contact angle of the toluene-derived SOM on a substrate measured by 3-D fluorescence confocal  
 14 microscope ranged from 80 - 100°. The relationship of viscosity and contact angle depends on the  
 15 ratio of the radius of a tube,  $R$ , to the radius of an inner hole,  $r$  (Grayson et al., 2015a).

16



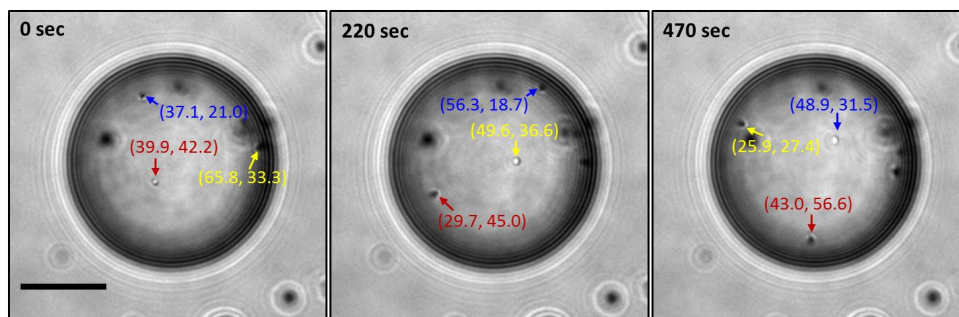
- 1 Table 3. Months when the afternoon RH in the 15 most populous megacities either does not go  
 2 below 45 % (at the 10<sup>th</sup> percentile level) or is 17% or lower (at the 10<sup>th</sup> percentile level). “None”  
 3 indicates the RH does not meet either of these criteria.

Megacity	Months when the afternoon RH (at the 10 <sup>th</sup> percentile level) does not go below 45 %	Months when the afternoon RH (at the 10 <sup>th</sup> percentile level) is 17 % or lower
Tokyo	Jun. – Sep.	none
Delhi	none	Mar. – Jun.
Shanghai	Jun. – Sep.	none
Mexico City	none	Jan. – May, Dec.
Sao Paulo	Jan.	none
Mumbai	May – Sep.	none
Osaka	Jul.	none
Beijing	none	Jan. – May, Nov. – Dec.
New York	none	none
Cairo	none	Mar. – May
Dhaka	Jun. – Oct.	none
Karachi	Jun. – Aug.	Jan. – Apr., Oct. – Dec.
Buenos Aires	none	none
Kolkata	May – Oct.	none
Istanbul	Jan. – Feb., Oct. – Dec.	none

4



1

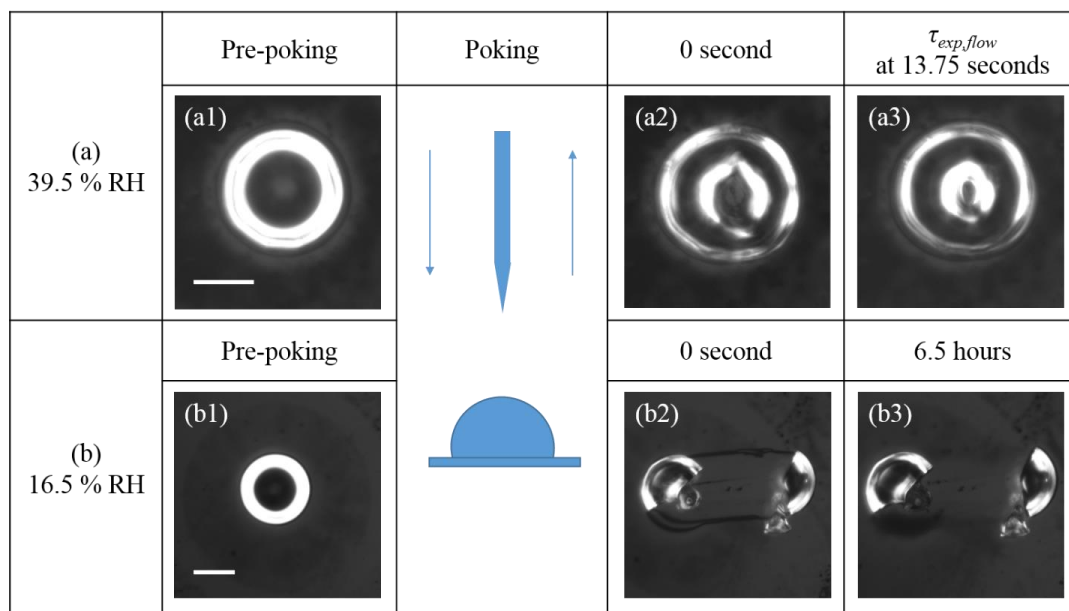


2

3 **Fig. 1.** Optical images from typical bead-mobility experiments for a toluene-derived SOM particle  
4 (Toluene sample 8 in Table 1) at 80% RH. Three different beads are labeled using colored arrows.  
5 The  $x$  and  $y$  coordinates of these beads are also indicated. Scale bar: 20  $\mu\text{m}$ .

6

7



1

2

3 **Fig. 2.** Optical images of pre-poking, poking, and post-poking from typical poke-flow experiments  
 4 on toluene-derived SOM particles (toluene sample 6) at (a) 39.5% RH and (b) 16.5% RH. Panel  
 5 a1 and b1; pre-poking, Panel a2 and b2: post-poking immediately after the needle has been  
 6 removed (time set = 0 s), Panel a3; the experimental flow time,  $\tau_{exp,flow}$ , where the diameter of hole  
 7 has decreased to 50% of its initial size, and Panel b3; particles shatter and do not flow over a period  
 8 of 6.5 h. Size bar: 20  $\mu\text{m}$ .

9

10

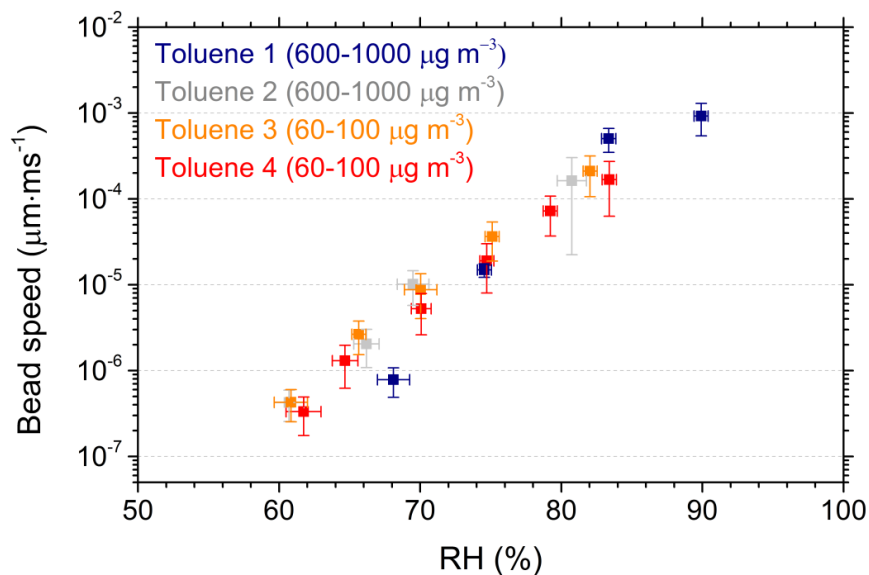
11

12

13

14

15

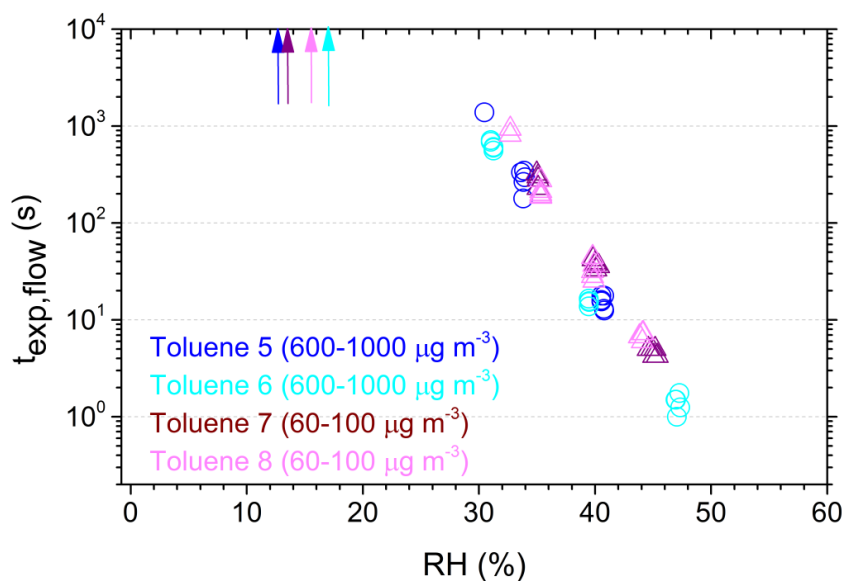


1

2

3 **Fig. 3.** Measured average bead speeds as a function of RH for different SOM samples (Toluene 1,  
4 2, 3, and 4, see Table 1). The bead speeds of 3 - 10 beads were used to determine a mean bead  
5 speed. The  $x$ -error bars represent the uncertainty in the RH measurements and the range of RH  
6 values in a given experiment. The  $y$ -error bars represent the standard deviation of the measured  
7 bead speeds.

8

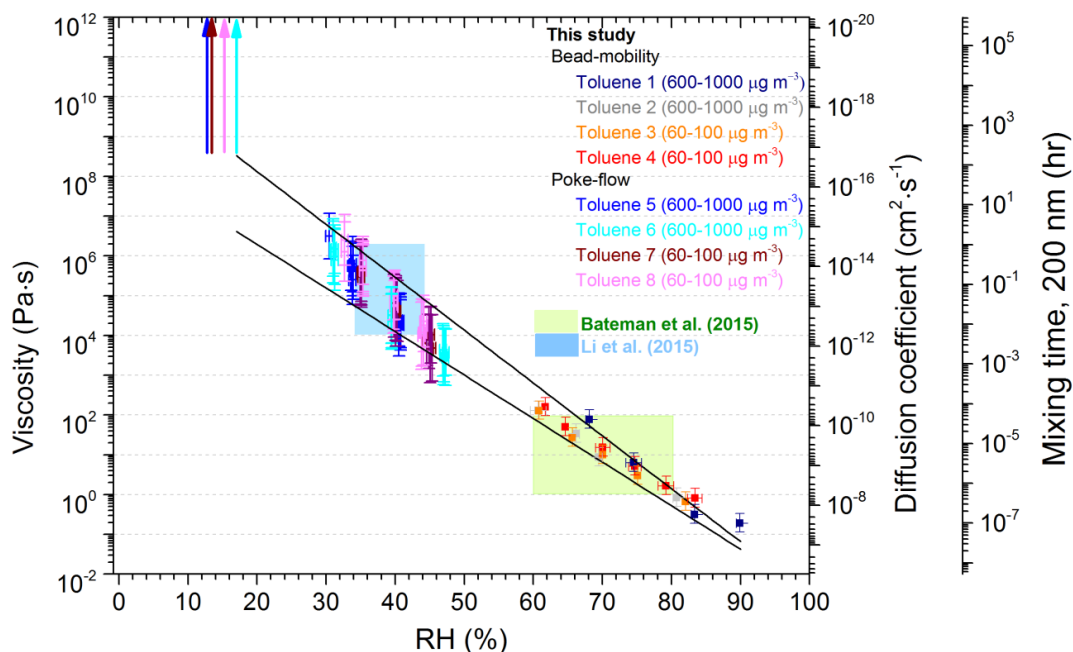


1

2

3 **Fig. 4.** Results from poke-flow experiments.  $\tau_{exp,flow}$ , where the diameter of hole has decreased to  
4 50% of its initial size, measured for the different samples (Toluene 5, 6, 7, and 8, see Table 1).  
5 The arrows indicate particles shattered at the given RH.

6

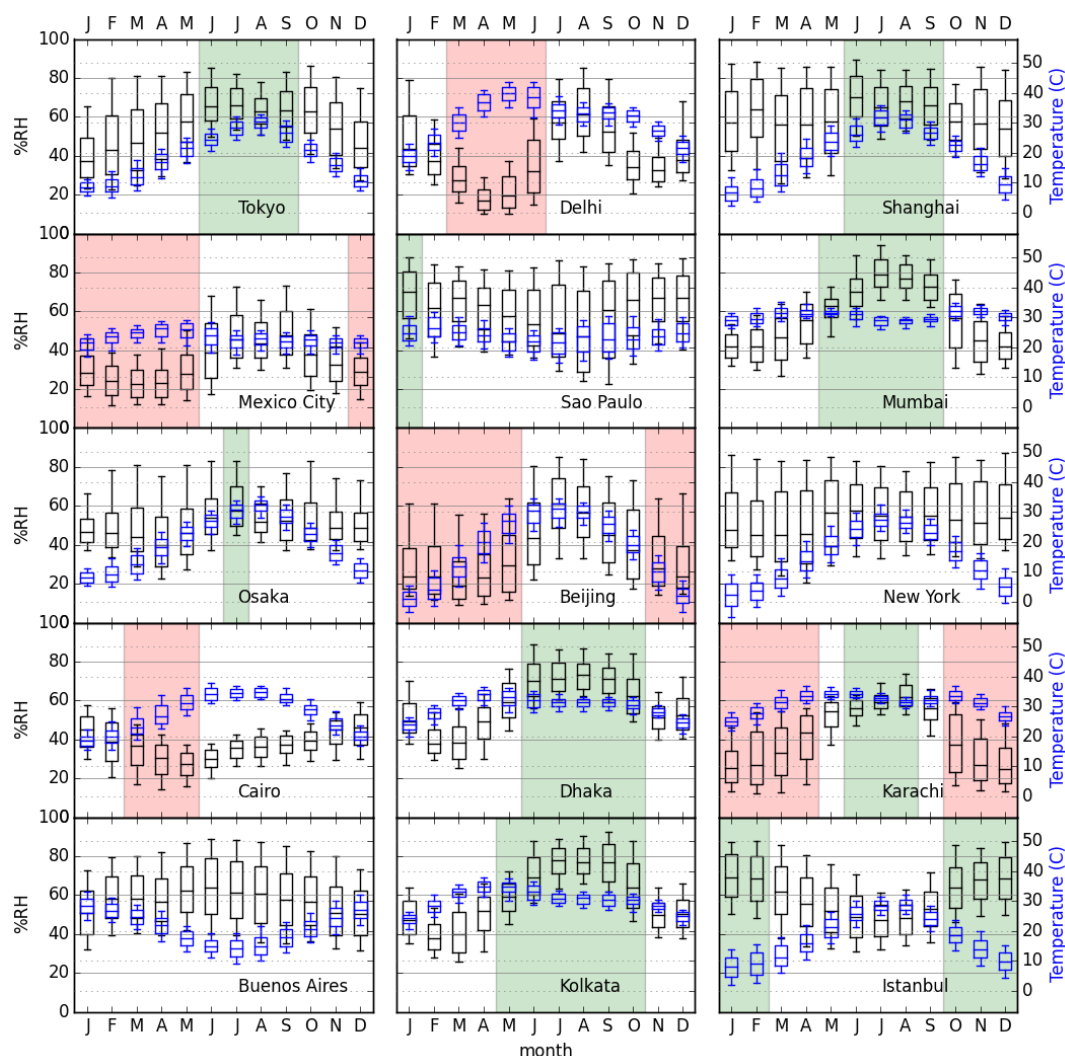


1

2

3 **Fig. 5.** Viscosities of toluene-derived SOM particles as a function of RH. For RH > 60% the  
 4 viscosities were determined from the mean bead speeds (see Fig. 3) and a calibration line (Song et  
 5 al., 2015). The y-error bars for RH > 60% represent the 95% prediction intervals from the  
 6 calibration line. For RH < 60% the viscosities were calculated from the  $\tau_{\text{exp, flow}}$  where y-error bars  
 7 represent the calculated lower and upper limits of viscosity using the simulations. The x-error bars  
 8 over the entire range of RH represent the range of RH values in a given experiments and the  
 9 uncertainty in the RH measurements. The right y-axes present calculated diffusion coefficients of  
 10 organic molecules in SOM using the Stoke-Einstein relation, and calculated mixing times within  
 11 200 nm particles due to bulk diffusion using Eq. (1). The black lines represent linear fits for the  
 12 RH vs. log(lower viscosities) ( $R^2 = 0.958$ ) and log(upper viscosities) ( $R^2 = 0.984$ ) from the entire  
 13 data set excluding the RH where particles cracked. Viscosity of toluene-derived SOM particles  
 14 from Bateman et al. (2015) (green box) and Li et al. (2015) (blue box) is also included.

15



1

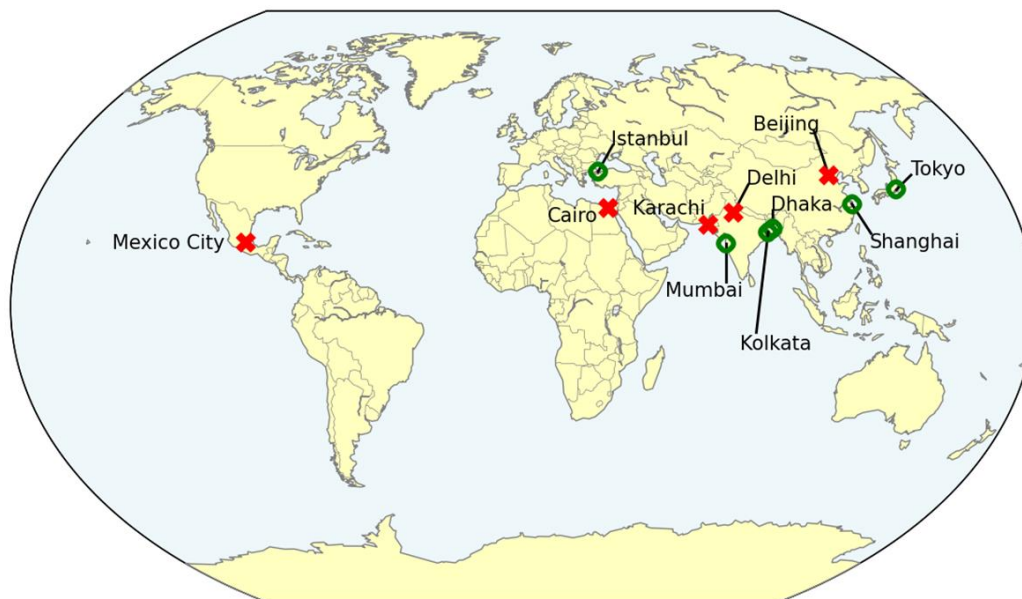
2

3 **Fig. 6.** Monthly average RH and temperature for the megacities of Tokyo, Delhi, Shanghai,  
4 Mexico City, São Paulo, Mumbai, Osaka, Beijing, New York, Cairo, Dhaka, Karachi, Buenos  
5 Aires, Kolkata, and Istanbul. For the stations, afternoon averages RH values (3-5 pm local time)  
6 were retrieved from NOAA's National Climate Data Center for the years from 2004 to 2014. Boxes  
7 show the median, 25<sup>th</sup> and 75<sup>th</sup> percentiles of 3-hr averages and the whiskers show the 10<sup>th</sup> and  
8 90<sup>th</sup> percentiles. Green shading indicates that the afternoon RH (at the 10<sup>th</sup> percentile level) does





- 1 not go below 45% RH. Red shading indicates that the afternoon RH (at the 10<sup>th</sup> percentile level)
- 2 is 17% or lower.
- 3



1

2

3 **Fig. 7.** Summary of conclusions reached after applying the results of the viscosities, diffusion  
4 coefficients, and mixing time of the toluene-derived SOM to the top 15 most populous megacities.  
5 Green circles indicates megacities where the afternoon RH at 10<sup>th</sup> percentile does not go below  
6 45 % RH for certain times of the year. In these cases, well-mixed particles can be assumed. Red  
7 crosses indicates megacities where the afternoon RH at 10<sup>th</sup> percentile is 17 % or lower for certain  
8 times of the year. In these cases, the particles may not be well-mixed in the afternoon for certain  
9 times of the year.